Received: 12 May 2020 | Revised: 17 July 2020 | Accepted: 27 July 2020

DOI: 10.1111/jace.17411

ORIGINAL ARTICLE

Journal of the American Ceramic Society

Intrinsic defects, Mo-related defects, and complexes in transition-metal carbide VC: A first-principles study

Jing Guo[1,2] | **Yunli Feng**[2] | **Cong Tang**[1] | **Xuejun Ren**[1]

[1]Department of Mechanical and Maritime Engineering, Faculty of Engineering and Technology, Liverpool John Moores University, Liverpool, UK

[2]College of Metallurgy and Energy, Hebei Key Laboratory of Modern Metallurgy Technology, North China University of Science and Technology, Tangshan, China

Correspondence
Jing Guo and Xuejun Ren, Department of Mechanical and Maritime Engineering, Faculty of Engineering and Technology, Liverpool John Moores University, Liverpool L3 5UG, UK.
Emails: guojing861014@163.com, j.guo@ljmu.ac.uk (J. G.); x.j.ren@ljmu.ac.uk (X. R.)

Funding information
H2020 Marie Skłodowska-Curie Actions, Grant/Award Number: 793114; National Natural Science Foundation of China, Grant/Award Number: 51674123

Abstract

Intrinsic defects and Mo-related defects in vanadium carbide VC, as well as the defect complexes between vacancies and Mo defects were investigated by means of first-principles calculations within the framework of density functional theory. In addition, Mo diffusion in VC was also studied using LST/QST method. The formation energies of defects have clearly shown that except C vacancy (V_C) all other point defects are not energetic favorable compared to perfect VC. V_C can exist in the lattice forming nonstoichiometric carbide VC_x ($x < 1$), and also can stabilize the Mo-related defects ($S_{Mo\text{-}V}$, $S_{Mo\text{-}C}$, and T_{Mo}). Free Mo atoms have the strong tendency to enter the already formed V_V and occupy the lattice position of V atoms. Meanwhile, Mo atom in C lattice ($S_{Mo\text{-}C}$) and interstitial Mo (I_{Mo}) atom can also enter the V_V position stabilizing the lattice structure. $S_{Mo\text{-}C} + V_V$ will transform into $S_{Mo\text{-}V} + V_C$ and $I_{Mo} + V_V$ will transform into $S_{Mo\text{-}V}$ during optimization, and large binding energy makes Mo atom tend to exist in the interstitial position. From the perspective of energy, Mo atom tends to diffuse through the interstitial position.

KEYWORDS

defect complex, diffusion, first-principles calculation, formation energy, intrinsic defect, vanadium carbide (VC)

1 | INTRODUCTION

Transition-metal carbide (TMC) is a kind of material with high melting point, high hardness, high thermal stability, and excellent corrosion resistance as well as special electrical, magnetic, and catalytic properties, which has been widely used in the field of machinery, mining, high-temperature structural components, nuclear materials, and new catalytic materials.[1-3]

Among all kinds of TMCs, vanadium carbide VC has attracted more attention all over the world due to its relatively low price of element V compared with W/Mo and relatively low formation energy, which is beneficial to control the precipitation of carbides.[4,5] As a strengthening phase, VC precipitates can improve the hardness and wear resistance of ferrous or nonferrous alloys.[6-9] Ultra-high hardness and strength can also be obtained if VC is applied into hard alloys, which are commonly used as tool materials to cut some difficult-to-machine materials.[10] In terms of material modification, VC can be used not only as coating materials but also as additive materials in coatings.[11,12]

Because of the extremely high melting point, VC normally precipitates at high temperature in metal materials,[13] the hard alloys which are made of VC need to be fabricated by high-temperature sintering,[14] and some special coatings containing VC will be manufactured by methods like thermal

spraying and thermal diffusion.[15] So some of the temperature-related point defects, such as vacancy, interstitial atoms, and impurity atoms, will exist inevitably in VC who has already gone through high-temperature treatment.[16,17] And the point defects have huge influence on the element diffusion in crystals as well as mechanical, electrical, magnetic, and optical properties of materials.[18-20] Therefore, it is of great significance to investigate the behavior of point defects in crystals.

Recently, the researches about point defects in TMCs have been reported from time to time. It is well-known that the point defects are the ones at the atomic scale, and it is difficult to study their effect in detail by conventional experimental methods. So first-principles calculations are commonly used by many researchers around the world. Burr et al[21] studied the formation and migration of point defects in tungsten carbide WC. Kong et al[22] revealed that the carbon vacancy is the dominant defect in hexagonal WC. Carbide TiC was chosen by Sun et al[23] to calculate the self-diffusion of Ti interstitial-based point defects and complexes. Razumovskiy et al[24] focused on a description of a complex vacancy behavior of the group IVb substoichiometric TMCs TiC, ZrC, and HfC carbides and found a strong tendency toward vacancy clustering in the carbides. DP Daroca et al[25] performed a study of the stability of different point defects in thorium carbide ThC, and demonstrated that C isolated vacancies are the most likely defects in ThC, whereas Th vacancies are highly unfavorable as compared to C ones. However, nearly all studies about the point defects in VC mainly focus on the nonstoichiometry caused by vacancy as well as the order and disorder problem,[26-29] and the analyses and discussion of different types of defects are rarely reported. So the first-principles method is adopted in this work to calculate the VC systems with different intrinsic defects (vacancy, substitution, and tetrahedral interstitial) and analyze their formation energy and electronic structure. In addition, other metal elements can exist in VC unavoidably during formation/fabrication process and diffuse into VC lattice at high temperature. For example, element Mo is often used as the binder in the preparation of hard alloys,[30] and Mo content is always found relatively high in VC in a self-designed novel Fe-based alloy by our group.[31] So Mo-related defects and the influence of impurity Mo atoms on the defects in VC, as well as Mo diffusion are also studied in this paper.

2 | CALCULATION DETAILS

First-principles calculations based on density functional theory (DFT)[32,33] with ultrasoft pseudopotentials were used to evaluate the intrinsic defects and Mo-related defects in VC supercell. The calculations were performed using Cambridge Sequential Total Energy Package (CASTEP). The valence electrons of V atom $3d^3 4s^2$ and C atom $2s^2 2p^2$ orbitals were treated by projector-augmented wave theory. The generalized gradient approximation (GGA) with Perdew-Burke-Ernzerho (PBE) functional was employed as exchange-correlation energy.[34,35] The Broyden-Fletcher-Goldfarb-Shanno (BFGS) algorithm was applied in relaxation process of models to optimize the structures. The energy, the maximum force, and maximum displacement were set as 5×10^{-6}eV/atom, 0.01 eV/Å, and 5×10^{-4} Å for the convergence tolerances, respectively. Based on convergence tests, which are shown in Figure S1, plane-wave cutoff energy was set at 380eV and Brillouin zone sampling was set at $6 \times 6 \times 6$ Monkhorst-Pack mesh for VC unit cell. LST/QST method was used to perform the migration barrier calculations to investigate the diffusion behavior of Mo atom.

The determination of supercell size was tested by calculating the formation energy of one V vacancy (V_V) or one C vacancy (V_C) existed in 8-atom, 16-atom, 32-atom, 64-atom, 96-atom, 144-atom, and 216-atom VC supercells, respectively (see Table S1 and Figure S2). Defect calculations were performed in a prerelaxed 64-atom supercell, consisting of $2 \times 2 \times 2$ replica of VC unit cell.

3 | RESULTS

3.1 | Intrinsic defects and Mo-related defects

3.1.1 | Lattice parameters

The models of three different intrinsic defects that may exist in VC supercell are established, which are (a) vacancies, (b) substitutions (antisite), and (c) interstitials (tetrahedral interstitials are considered here). Each intrinsic defect contains two different types considering the existence of V and C atom in the supercell. So first-principles calculations about intrinsic defects are performed in VC supercell with V vacancy (V_V), C vacancy (V_C), V substitution (Sv), C substitution (S_C), V interstitial (Iv), and C interstitial (I_C), respectively. Only one atom defect is considered among the intrinsic defects throughout. Figure 1 shows the structures of VC with different intrinsic defects. Note that only unit cells are displayed here for clarity.

Mo-related defects in VC supercell contain two different types, one is Mo substitutions and the other is Mo interstitial. Mo substitutions refer to the defects that one V or C atom is replaced by one Mo atom in the structure, which are represented by $S_{Mo\text{-}V}$ and $S_{Mo\text{-}C}$ in this paper. While Mo interstitial defect (I_{Mo}) is similar to I_V and I_C, which means one Mo atom enters into the tetrahedral interstitial site in crystal structure. The corresponding structure models are shown in Figure 2.

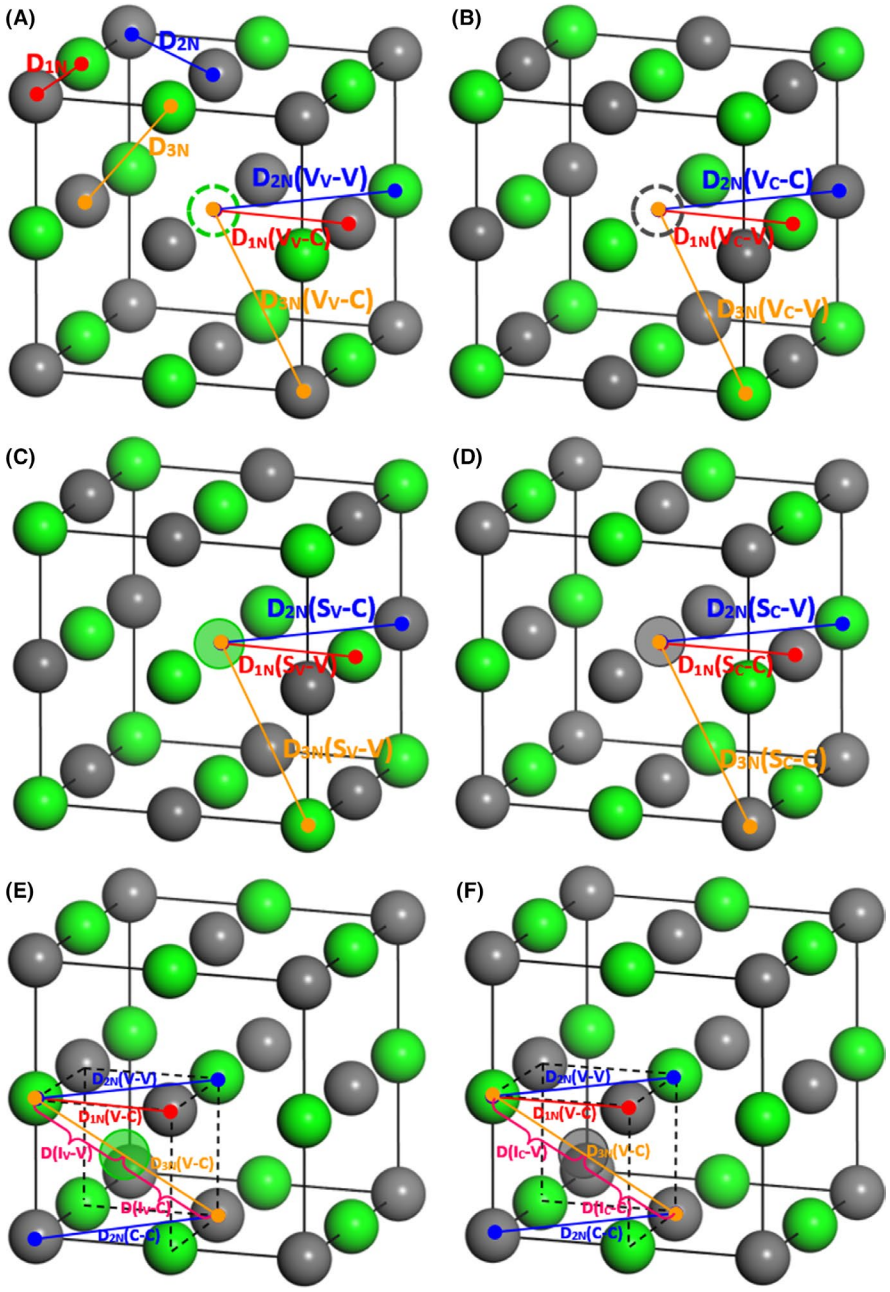

FIGURE 1 Schematic diagram of VC structure with (A) V vacancy (V_V), (B) C vacancy (V_C), (C)V substitution (Sv), (D) C substitution (S_C), (E) V interstitial (Iv), and (F) C interstitial (I_C). Green and gray balls represent V and C atoms; Green and gray dashed circles in (A) and (B) indicate V_V and V_C; Green and gray semitransparent balls in (C) and (D) are Sv and Sc, whereas in (E) and (F) are Iv and Iv [Color figure can be viewed at wileyonlinelibrary.com]

The distances of atoms in the supercell near defect in supercell are collected and listed in Table 1. For perfect VC supercell, D_{1N}, D_{2N}, and D_{3N} represent the first, second, and third nearest distance between atoms, which can be seen in Figure 1A. For VC supercell with V_V, V_C, S_V, S_C, $S_{Mo\text{-}V}$, and $S_{Mo\text{-}C}$ defects, D_{1N}, D_{2N}, and D_{3N} represent the distance from the defect to the first, second, and third nearest atom. For VC supercell with I_V, I_C, and I_{Mo}, D_{1N}, D_{2N}, and D_{3N} represent the first, second, and third nearest distance between atoms in the cube (the part surrounded by dashed lines in Figures 1E,F, and 2C) where the interstitial atom locates in the center. Detailed figures explaining D_{1N}, D_{2N}, and D_{3N} for different defect situations that listed in Table 1 can also be found in Figures 1 and 2.

From Table 1, although V_V and V_C both belong to vacancy defect, the effect of existence of V and C vacancy on the structure lattices differs from each other. V vacancy mainly affects D_{2N}. In this case, the second nearest distance D_{2N} is the distance from V_V to V atoms nearby, which is indicated by (V_V-V) after the value in Table 1. The distance change compared to perfect system $\Delta D_{2N}/D_{2N}^{per}$ for V_V is the largest, −2.38%, but still much smaller than the largest distance change $\Delta D_{1N}/D_{1N}^{per}$ for V_C, 7.17%. Interestingly, the distance change values for V_V distribute more evenly and only $\Delta D_{2N}/D_{2N}^{per}$ is larger than values for V_C, but the volume change (−0.548%) for VC supercell with V_V is larger than that (0.119%) with V_C. In addition, when V vacancy exists in the supercell, D_{1N}, D_{2N}, and D_{3N} all become smaller compared to the perfect system resulting in the shrinkage of the

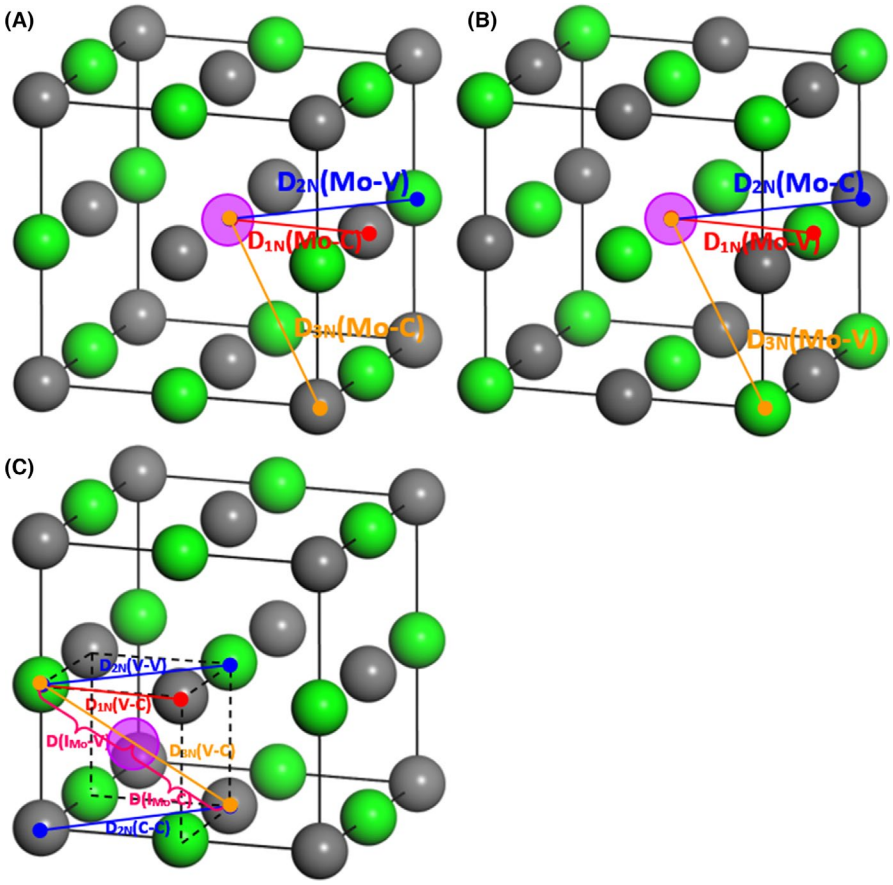

FIGURE 2 Schematic diagram of VC structure with Mo-related defects: (A) Mo substitutes V (S_{Mo-V}), (B) Mo substitutes C (S_{Mo-C}), and (C) Mo interstitial (I_{Mo}). Green and gray balls represent V and C atoms; Purple semi-transparent balls in (A), (B), and (C) are S_{Mo-V}, S_{Mo-C}, and I_{Mo} [Color figure can be viewed at wileyonlinelibrary.com]

TABLE 1 Distance (D_{1N}, D_{2N}, and D_{3N}, Å) from the atom/defect to the first, second, and third nearest atom in VC supercells with/without defects after optimization; V_0 and V (Å^3) are the volume of perfect VC supercell and supercells with defect; $\Delta V/V_0$ (%) is the volume change between VC supercell with defect and perfect system, $\Delta V = V - V_0$

Supercell	D_{1N}	D_{2N}	D_{3N}	V	$\Delta V/V_0$
Perfect	2.078	2.939	3.601	574.632 (V_0)	
V_V	2.058 (V_V-C)	2.869 (V_V-V)	3.585 (V_V-C)	571.483	−0.548
V_C	2.227 (V_C-V)	2.920 (V_C-C)	3.555 (V_V-V)	575.316	0.119
S_V	2.335 (S_V-V)	2.938 (S_V-C)	3.599 (S_V-V)	586.664	2.094
S_C	1.880 (S_C-C)	2.947 (S_C-V)	3.583 (S_C-C)	570.570	−0.707
I_V	2.427 (V-C)	3.725 (V-V) 3.079 (C-C)	4.166 (V-C = I_V-V + I_V-C) * I_V-V = 2.281, I_V-C = 1.885	598.553	4.163
I_C	2.187 (V-C)	3.406 (V-V) 2.699 (C-C)	3.739 (V-C = I_V-V + I_V-C) * I_C-V = 2.086, I_C-C = 1.653	581.139	1.132
S_{Mo-V}	2.123 (Mo-C)	2.971 (Mo-V)	3.607 (Mo-C)	577.881	0.565
S_{Mo-C}	2.349 (Mo-V)	2.955 (Mo-C)	3.609 (Mo-V)	590.112	2.694
I_{Mo}	2.511 (V-C)	3.843 (V-V) 3.201 (C-C)	4.313 (V-C = I_{Mo}-V + I_{Mo}-C) * I_{Mo}-V = 2.353, I_{Mo}-C = 1.960	605.825	5.428

crystal structure, which obviously seems reasonable. However, after one C atom is removed from the lattice, D_{1N} from V_C to the nearest V atoms increases instead, which directly leads to slight lattice expansion.

For substitution defect Sv and S_C, one larger V atom substitutes smaller C atom resulting in the increase in supercell volume, whereas one smaller C atom substitutes larger V atom resulting in the decrease in supercell volume, both of which are understandable. Only minor change in D_{2N} and D_{3N} can be seen compared to the perfect system, especially for S_V. D_{1N} become larger than that of perfect system for S_V, and the distance change $\Delta D_{1N}/D_{1N}^{per}$ reaches 12.37%, whereas D_{1N} for S_C decreases compared to

perfect system with the distance change in −9.53%, which shows that substitution atom mainly influence its nearest atom position.

When a new V atom is added in the tethahedral site of the lattice (cubic part represented by dashed lines in Figure 1E), eight vertices of the cube where V atom is located in the center all expand outward, which make D_{1N}(V-C) and D_{3N}(V-C) both increase. Additionally, the displacement of V atoms at the vertex is larger than that of C atoms, so the value of D_{2N}(V-V) is greater than that of D_{2N}(C-C). When a new C atom is added into the lattice, four vertices containing V atoms expand outwards, whereas four C atoms contract inwards, which make D_{2N}(V-V) increase and D_{2N}(C-C) decrease. Finally, the combined result of V and C movement leads to slight increase in both D_{1N}(V-C) and D_{3N}(V-C). Overall, when V atom is added into the tetrahedral site, the lattice changes more obviously than C addition, mainly because of the larger radius of V atom resulting in the severe lattice distortion. The larger volume change for I_V also confirms the above conclusion.

Mo is also a transition-metal element with an atomic radius similar to but slightly larger than V, as well as same bonding between Mo and C atom with V-C bond, which results in a little larger D_{1N}, D_{2N}, and D_{3N} values than perfect system if one V atom is replaced by Mo atom with volume change of only 0.565%. When one Mo atom substitutes C atom in the structure, the situation is totally different from $S_{Mo\text{-}V}$. V-Mo-V atoms instead of V-C-V atoms arrange in a row along x, y, and z directions and the nearest V atoms around Mo atom move outwards finally causing the volume expansion. The introduction of Mo atom into the tethahedral position has the similar result to I_V. D_{1N}, D_{2N}, and D_{3N} values all become much larger than the perfect structure, and the displacement of C atoms at the vertex is smaller than that of V atoms. Due to the larger radius of Mo than V, all the values for I_{Mo} listed in Table 1 are larger than I_V, the volume change is the largest among all the supercells with defects.

3.1.2 | Formation energy

In this paper, two kinds of formation energy—(a) formation energy for intrinsic defects, (b) formation energy for bulk material with defects—are considered to investigate the stability of VC structure after the defects being introduced.

The formation energy for intrinsic defects can be expressed by Eq.(1)-(3) [36,37]:

For vacancy defect:

$$E_V^{def} = E(N-1) - E_{per}(N) + E(A)\ (A = V \text{ or } C) \quad (1)$$

For substitution defect:

$$E_S^{def} = E(N) - E_{per}(N) + E(B) - E(A)\ (A = V \text{ or } C,\ B = C \text{ or } V) \quad (2)$$

For interstitial defect:

$$E_I^{def} = E(N+1) - E_{per}(N) - E(A)\ (A = V \text{ or } C) \quad (3)$$

where E^{def} is formation energy for intrinsic defects, the subscript V, S, I here represent vacancy, substitution, and interstitial defect; E(N − 1), E(N), and E(N + 1) are the relaxed total energy of supercell including one vacancy, substitution, or interstitial defect; $E_{per}(N)$ is the relaxed total energy of the corresponding ideal supercell crystal; E(V) and E(C) are the energy per V atom in pure cubic V crystal and C atom in graphite crystal, respectively.

The formation energy of defects is also close related to the chemical potential that may change in different chemical environments. If chemical potential is considered here, the formation energy of intrinsic defects in VC can be computed as following expression:

$$E_f = E_{tot}(\text{defect}) - E_{per} - \sum_j \Delta n_j \mu_j \quad (4)$$

where E_{tot} (defect) is the relaxed total energy of supercell including intrinsic defects; E_{per} is the relaxed total energy of the perfect supercell; n_j represents the atom number of type j removed from ($\Delta n_j > 0$) or added ($\Delta n_j < 0$) to crystal lattice when defect is formed, and μ_j is corresponding chemical potential for alloy element.

In order to make VC compound stable, $\Delta\mu_V$ and $\Delta\mu_C$ should satisfy the following equation:

$$\Delta\mu_V + \Delta\mu_C = \Delta H(VC) \quad (5)$$

where ΔH(VC) in Equation (5) is the formation enthalpy of VC per unit cell in solid phase; $\Delta\mu_V$ and $\Delta\mu_C$ are the relative chemical potentials for V and C, which can be denoted as:

$$\Delta\mu_V = \mu_V - \mu_V^{solid} \quad (6)$$

$$\Delta\mu_C = \mu_C - \mu_C^{solid} \quad (7)$$

where μ_V^{solid} and μ_C^{solid} are the energies of pure V and C in their standard states, respectively.

To avoid precipitation of element solid V and C, the relative chemical potentials should be restricted by the following equations:

$$\Delta\mu_V \le 0 \quad (8)$$

$$\Delta\mu_C \le 0 \quad (9)$$

From the binary phase diagram of V-C system, the VC phase equilibrates with its neighboring V_2C phase under

V-rich condition. To avoid the formation of V_2C, chemical potentials must also be bounded by the following equation:

$$\Delta\mu_V + \Delta\mu_C \le \Delta H\left(V_2C\right) \tag{10}$$

The chemical potential ranges for V and C are determined according to above equations and shown in Figure 3.

The formation energy for bulk material with defects is presented as follows:

$$E^{bulk} = \frac{E\left(VxCy\right) - xE\left(V\right) - yE\left(C\right)}{x+y} \tag{11}$$

where E^{bulk} is formation energy for bulk material with defects; E(VxCy) is the relaxed total energy of supercell including defects; x and y are the number of V and C atom in corresponding supercell.

The formation energy for Mo-related defects can be expressed as follows:

For Mo substitution defect:

$$E^{def}_{Mo\text{-}S} = E\left(N,\ Mo\right) - E_{per}\left(N\right) - E\left(Mo\right) + E\left(A\right)\ \left(A = V \text{ or } C\right) \tag{12}$$

For Mo interstitial defect:

$$E^{def}_{Mo\text{-}I} = E\left(N+1,\ Mo\right) - E_{per}\left(N\right) - E\left(Mo\right) \tag{13}$$

where the subscript Mo-S, Mo-I in E^{def} represent Mo substitution and Mo interstitial defect; E(N, Mo) and E(N + 1, Mo) are the relaxed total energy of supercell including Mo substitution or Mo interstitial defect; E(Mo) is the energy per Mo atom in pure hexagonal Mo crystal.

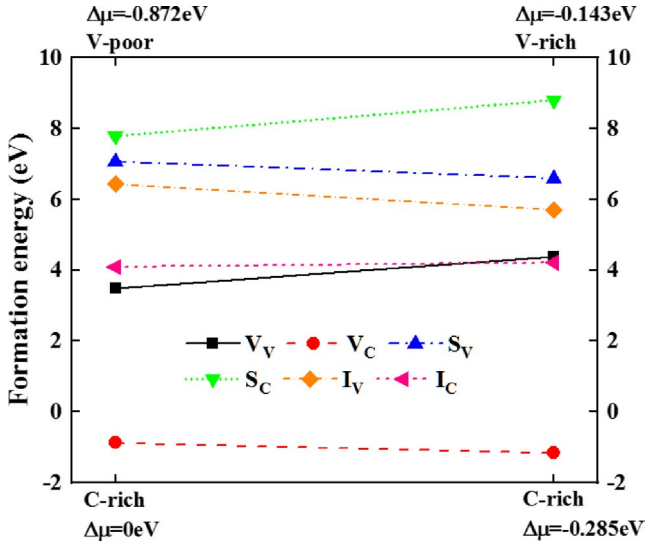

FIGURE 3 Formation energies of intrinsic defects as function of the chemical potentials [Color figure can be viewed at wileyonlinelibrary.com]

The formation energy for bulk material with Mo-related defects is presented as follows:

$$E^{bulk}_{Mo} = \frac{E\left(VxCyMo\right) - xE\left(V\right) - yE\left(C\right) - E\left(Mo\right)}{x+y+1} \tag{14}$$

where E^{bulk}_{Mo} is formation energy for bulk material with Mo-related defects; E(VxCyMo) is the relaxed total energy of supercell including Mo-related defects.

From Figure 3, it can be seen that if chemical potentials are considered, the formation energies for different intrinsic defects are not a fixed value, but within a certain range. In general, the formation energies for vacancy defect are the smallest, then followed by interstitial and substitution defects, and no obvious overlapping can be observed for their value ranges. So the formation energies of defects that calculated by Equations (1)-(3), (12)-(13) without consideration of chemical potentials are analyzed in this section. Table 2 lists the results of formation energy for all supercells with different kinds of defects. The results of formation energy for intrinsic defects are in agreement with the results of formation energy for bulk material with defects. For a specific point defect, larger formation energy for the defect corresponds to larger formation energy for bulk material with defect. The more negative the energy, the easier it is to form such a defect. Among all intrinsic and Mo-related defects, V_C has the lowest formation energy values indicating that V_C is the most stable defect in the structure, which is already demonstrated by the researchers around the world,[38,39] and all other point defects are not energetic favorable compared to perfect VC.

As the extraneous defects, Mo-related defects are less stable than intrinsic ones in VC structure in general, such as $S_{Mo\text{-}C}$ and I_{Mo}, but $S_{Mo\text{-}V}$ is an exception. The formation energy of $S_{Mo\text{-}V}$ is only larger than that of V_C and perfect cell showing relatively higher probability to exist in the crystal cell. This

TABLE 2 Formation energy (eV) of intrinsic defects and bulk material with defects

	Formation energy	
Supercell	**Point defect**	**Bulk material**
Perfect		−0.436
V_V	4.365	−0.366
V_C	−0.880	−0.451
S_V	6.204	−0.338
S_C	8.672	−0.290
I_V	5.571	−0.349
I_C	4.099	−0.367
$S_{Mo\text{-}V}$	1.141	−0.412
$S_{Mo\text{-}C}$	6.892	−0.322
I_{Mo}	8.589	−0.294

indicates that when element Mo is present in the alloy, Mo atoms seems more likely to enter into VC carbide and occupy the lattice position of V atoms to form extraneous Mo-related defects, but the premise is that V_V should be formed firstly. It is known from the formation energies for V_V in Table 2 that the formation ability of V_V is only at an intermediate level, and the structure with $S_{Mo\text{-}V}$ still has higher formation energy than perfect cell, so the existence of $S_{Mo\text{-}V}$ is just a matter of probability, which does not reveal that $S_{Mo\text{-}V}$ must exist in the system.

3.1.3 | Electronic structures

Figure 4 shows the electron density difference distribution for VC supercell with intrinsic defects along specific direction. The value of electron density difference around V atoms in the structure is negative, whereas the value is positive for C atoms, which means that V atoms lose the electron and C atoms gain electron. When V_V exists in the supercell (see Figure 4A), the charge around C atoms in the nearest position mainly transfers to V atoms in the second nearest position, that isthe nearest C atoms form bonds with the second nearest V atoms around V_V, but the electron-gaining capacity of the nearest C atoms around the vacancy is slightly weaker than that of other normal C positions in the structure (see Table 3). If there is V_C in the supercell shown in Figure 4B, the V atoms in the nearest position mainly bond with the fourth nearest C atoms rather than the second nearest C atoms around V_C, resulting in the larger D_{1N} (2.227Å) than that of perfect structure. Meanwhile, a circular region on the side of V_C exists close to the nearest V atoms, which has strong ability to gain electrons.

The existence of S_V directly leads to the appearance of the circular area with positive differential charge density along ±x and ±y around the antisite V atom showing a very strong tendency to gain electrons according to Figure 4C. Similar to the situation of V_C, there also exists a circular area with strong ability to gain electrons for four nearest V atoms, which are found to bond with the fourth nearest C atoms. The above-mentioned strong electron-gaining areas may result in the smaller atomic charge around defect V and its nearest V atoms in VC supercell. From Table 3, the atomic charge value −0.05 of substitutional C atom is much smaller than normal C atoms in the supercell showing very small tendency to gain electrons, which can be easily observed through the color difference between defect atom and normal C atoms in Figure 4D. Meanwhile, the nearest C atoms are mainly bonded with the second nearest V atoms after original V atom is substituted by C atom.

When V atom is added in the interstitial position, the interstitial V atom itself nearly shows no electron transfer (charge 0.01), which seems not consistent with electron density difference distribution in Figure 4E. Strong V-C bonds between interstitial V atom and nearest C atoms can be observed clearly. Additionally, a circular region near I_V along

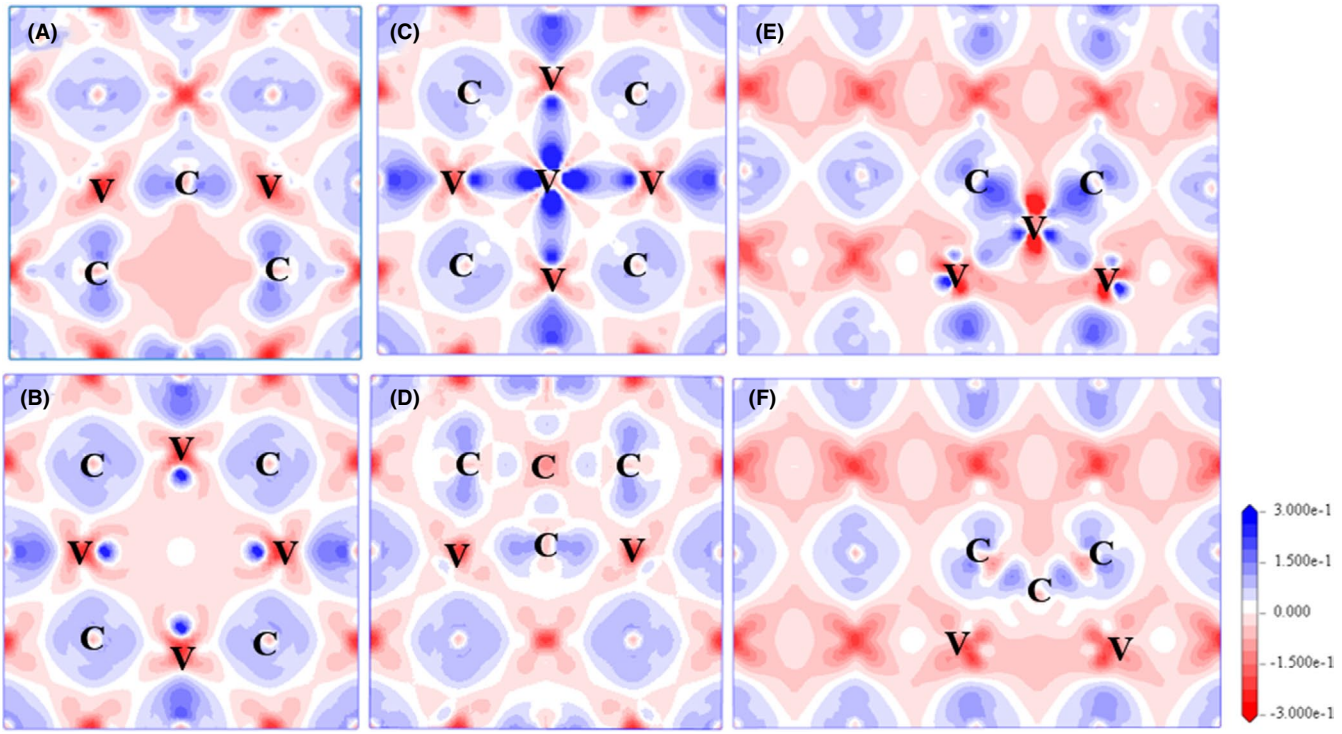

FIGURE 4 Electron density difference distribution for VC supercell with intrinsic defects of (A) V_V, (B) V_C, (C) Sv, and (D) S_C along (100) plane, as well as (E) Iv and (F) I_C along (110) plane [Color figure can be viewed at wileyonlinelibrary.com]

TABLE 3 Atomic charge (e) of defect atom and the first (1N), second (2N), and third (3N) nearest atoms in VC supercells with defects. In perfect VC structure, atomic charge for V and C atom is 0.6 and −0.6, respectively

	Atomic charge			
Defect	Defect atom	1N	2N	3N
V_V		C −0.53	V 0.60	C −0.61
V_C		V 0.55	C −0.61	V 0.57
S_V	V 0.42	V 0.48	C −0.61	V 0.60
S_C	C −0.05	C −0.49	V 0.62	C −0.60
I_V	V 0.01	V 0.59 C −0.62		
I_C	C −0.43	V 0.72 C −0.57		
S_{Mo-V}	Mo 0.23	C −0.60	V 0.63	C −0.60
S_{Mo-C}	Mo 0.03	V 0.55	C −0.61	V 0.60
I_{Mo}	Mo −0.51	V 0.67 C −0.61		

V-V bonds causes the tendency of sharing electrons. Maybe the combination of losing electrons in V-C bonds and sharing electrons in V-V bonds leads to unobvious electron transfer for interstitial V atom. The addition of interstitial C atom is the only condition that makes V atoms nearby lose more electrons than perfect structure among all intrinsic defects. This is because the nearest V atoms not only bond with the normal C atoms but also bond with the interstitial C atom (see Figure 4F).

Figure 5 shows the electron density difference distribution for VC supercell with Mo-related defects along specific direction. When one Mo atom substitutes V atom in VC structure, it can be found in Figure 5A that Mo atom not only bonds with all nearest C atoms, which gain electrons with atomic charge of −0.6, but also bonds with the second nearest V atoms and shares electrons with them. So higher atomic charge of V atoms (0.63) results in the lower value of 0.23 for substituted Mo. After one C atom is substituted by Mo atom (see Figure 5B), Mo atom forms bond with the second nearest C atom with longer bond length than Mo-C bond in situation of S_{Mo-V}, which indicates that the ability of Mo losing electrons is getting worse. Meanwhile, Mo atom shares electrons with the nearest V atoms showing the capability of gaining electrons to some extent. So Mo atom shows no obvious electron transfer (charge 0.03) in Table 3. From Figure 5C, electron density difference distribution for I_{Mo} is similar to that of I_V, but the atomic charges for interstitial atom of V (I_V) and Mo (I_{Mo}) in Table 3 are totally different. Interstitial Mo atom mainly bond with the nearest C atoms forming strong Mo-C bonds with bond length of 1.96nm, which is similar to the reaction of interstitial V atom and nearest C atoms in Figure 4E. However, Mo and V are both metallic atoms, but with different abilities of losing electrons, which make Mo atom exhibit the characteristic of gaining electrons.

3.2 | Defects complexes

When two defects exist in the crystal structure at the same time, the equation for binding energy of defect-defect interaction can be expressed as follows[40]:

$$E_{\text{defect-defect}} = E(N, \text{defect1}) + E(N, \text{defect2}) - E(N, 2\text{defects}) - E_{\text{per}}(N) \quad (15)$$

where $E(N, \text{defect 1})$ and $E(N, \text{defect 2})$ are the relaxed total energy of supercell containing one defect in the system; $E(N, 2\text{ defects})$ is the relaxed total energy of supercell including two defects at the same time.

After calculation according to Equation (15), the negative value represents the exothermic reaction between two defects indicating that these two defects repel each other, whereas the positive value shows the reaction of two defects is endothermic, which means the two defects attract each other.

It is well-known that vacancy-type defects are commonly seen in crystal structures, especially V_C defect, which has

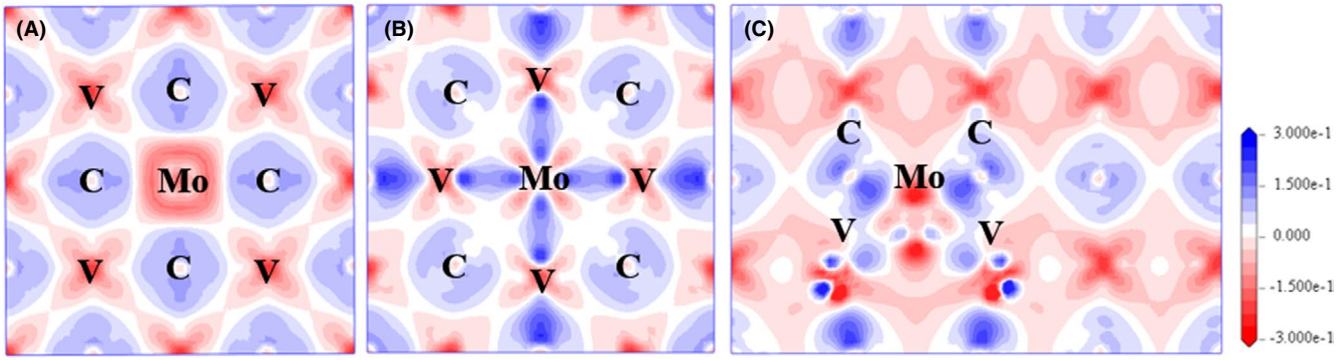

FIGURE 5 Electron density difference distribution for VC supercell with Mo-related defects of (A) S_{Mo-V} and (B) S_{Mo-C} along (100) plane, as well as (C) I_{Mo} along (110) plane [Color figure can be viewed at wileyonlinelibrary.com]

already been demonstrated in this paper. Moreover, vacancy-assisted diffusion is one of the most basic diffusion mechanisms, and alloy element atoms can leave their previous site and migrate to a nearby vacant lattice site to achieve diffusion inside the crystal. So in this section, only the combination of Mo-related defects and vacancy defect is considered and analyzed here, which can lay a theoretical foundation for the subsequent diffusion research in next section.

3.2.1 | Mo substitution-Vacancy defects

Mo substitution-Vacancy defects, which are presented by $S_{Mo\text{-}V} + V_V$, $S_{Mo\text{-}V} + V_C$, $S_{Mo\text{-}C} + V_V$, and $S_{Mo\text{-}C} + V_C$, can obtained by replacing one V or C atom by one Mo atom to form $S_{Mo\text{-}V}$ and $S_{Mo\text{-}C}$ defect first and deleting the nearest V or C atom of $S_{Mo\text{-}V}$ or $S_{Mo\text{-}C}$ defect subsequently.

For $S_{Mo\text{-}V} + V_V$ and $S_{Mo\text{-}V} + V_C$, the atoms on the (001) plane where both substituted Mo atom and V/C vacancy locate do not change too much after structure optimization (see Figure 6A,B), and the volume expansion caused by Mo substitution with larger atomic radius and volume shrinkage caused by V/C vacancy both contribute to unobvious volume change of supercell with $S_{Mo\text{-}V} + V_V$ and $S_{Mo\text{-}V} + V_C$ defects in Table 4. As a metal atom, Mo occupies the place where another metal atom V locates in supercell making $S_{Mo\text{-}V}$ defect very stable, so the values of binding energy between $S_{Mo\text{-}V}$ and V_V/V_C are both very small showing the weak attraction between them. However, due to the existence of the most stable V_C defect in the supercell, the formation energies for $S_{Mo\text{-}V} + V_C$ is much smaller than those of $S_{Mo\text{-}V} + V_V$ and almost the same with perfect structure.

For $S_{Mo\text{-}C} + V_V$, the whole optimization process consists of 34 steps, and Mo atom has completely entered into V vacancy at Step 13. Meanwhile, Mo atom can perfectly fit into the crystal lattice even undergoing obvious displacement but still doesn't affect the positions of other atoms in the supercell observed from (001) plane in Figure 6C. This indicates the $S_{Mo\text{-}C} + V_V$ complex is not stable and does not exist in the lattice, so it is meaningless to calculate the corresponding binding energy between $S_{Mo\text{-}C}$ and V_V. When $S_{Mo\text{-}C}$ and V_C defects both exist in the structure (see Figure 6D), Mo atom moves from original substituted position to the interstitial position in the lattice resulting in the formation of two C vacancies existed simultaneously. After Mo atom enters into the interstitial position, the nearest V atoms around Mo move outward and the displacement of atoms in other positions has also changed significantly, which lead to the volume increase in structure.

Mo interstitial-Vacancy defects

Mo interstitial-Vacancy defects $I_{Mo} + V_V$ and $I_{Mo} + V_C$ can be formed by introducing one Mo atom into the tetrahedral

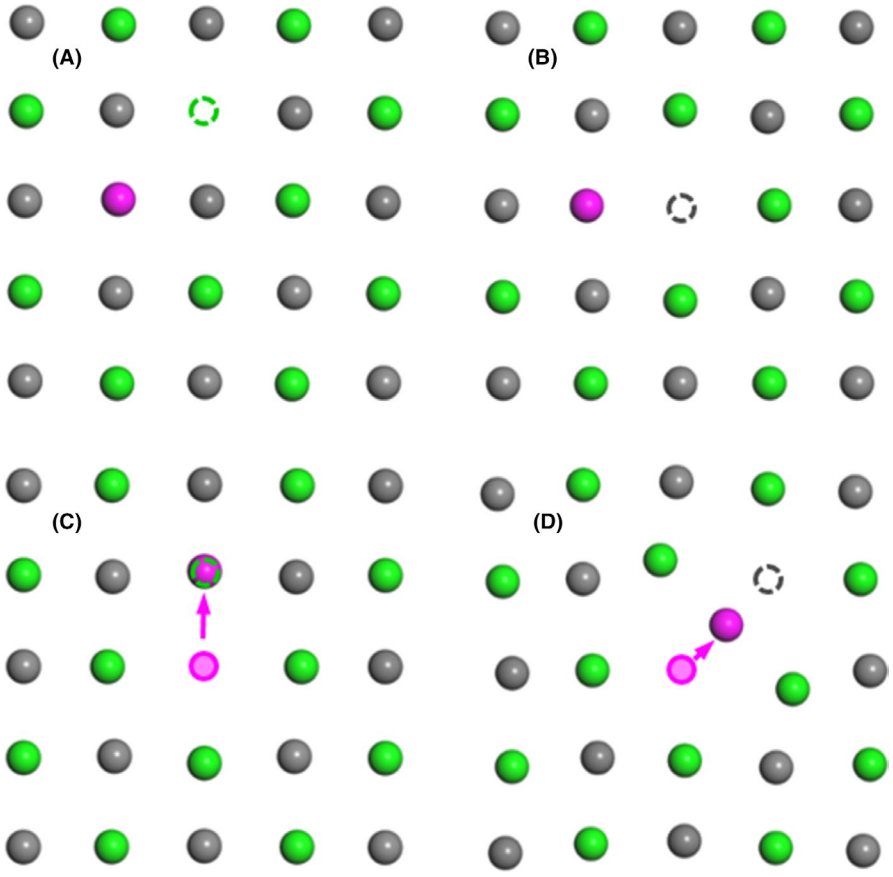

FIGURE 6 Structure model after optimization along (001) plane of VC supercell with (A) $S_{Mo\text{-}V} + V_V$, (B) $S_{Mo\text{-}V} + V_C$, (C) $S_{Mo\text{-}C} + V_V$, and (D) $S_{Mo\text{-}C} + V_C$. The green and gray balls represent V and C atoms, the dashed green and gray circles represent the original place where V_V and V_C locate, and the semitransparent purple balls represents the original place where substituted Mo atom locates [Color figure can be viewed at wileyonlinelibrary.com]

TABLE 4 Volume (V, Å^3), formation energy (eV), and binding energy (eV) of different defect complexes

Supercell	V	Formation energy		Binding energy
		Point defect	Bulk material	
Perfect	574.632 (V_0)		−0.436	
$S_{Mo-V} + V_V$	575.128	5.339	−0.352	0.188
$S_{Mo-V} + V_C$	577.869	0.103	−0.435	0.160
$S_{Mo-C} + V_V$	577.936	0.091	−0.435	—
$S_{Mo-C} + V_C$	589.523	3.316	−0.384	2.697
$I_{Mo} + V_V$	578.048	1.022	−0.414	—
$I_{Mo} + V_C$	592.777	4.547	−0.359	3.163

interstitial position and then removing the nearest V or C atom around interstitial Mo.

When both of I_{Mo} and V_V exist in the supercell (see Figure 7A), as the optimization proceeds, interstitial Mo atom moves in the direction of V_V and almost completely enters into the vacancy at Step 15 forming a perfect crystal lattice without interstitial defect anymore. During this process, the neighboring atoms around Mo first deviate from the original lattice position, and as Mo atom enters the lattice they gradually move back to the original position again. Finally, no obvious displacement can be observed for each atom in the lattice. The situation of $I_{Mo} + V_V$ is found similar to that of $S_{Mo-C} + V_V$, which means no such defect complex exists stably in VC structure, so no binding energy value was calculated and listed in Table 4.

If one of the nearest C around interstitial Mo was deleted instead of V atom, $I_{Mo} + V_C$ defect can be formed shown in Figure 7B. During the optimization process, Mo atom moves toward C vacancy but never enters into the lattice completely, and the surrounding atoms around Mo have shifted significantly until the final step, especially the surrounding V atoms near Mo. After Step. 16, nearly all atoms have no obvious change in position. Eventually, interstitial Mo atom locates near to C vacancy instead of staying in the center of tetrahedral interstitial position. Moreover, relatively small binding energy in Table 4 manifests a certain level of attraction between I_{Mo} and V_C, but the attraction is not strong enough to make the interstitial Mo totally enter into the lattice, which leads to the largest structure volume among all the defect complexes and larger formation energies indicating relatively unstable existence of $I_{Mo} + V_C$ defect.

3.3 | Mo atom diffusion

In this section, two diffusion ways which are commonly seen in the study of atomic diffusion behavior are considered here: (a) Interstitial diffusion and (b) Vacancy-assisted diffusion.

When interstitial Mo defect exists in the crystal alone, Mo atom diffuses through the interstitial site. In this section, we only consider one interstitial Mo atom jumps into the nearest interstitial site. Figure 8A shows the diffusion path and obtained energy profile for Mo interstitial diffusion. The energy profile is in symmetry and saddle point locates at halfway position from initial interstitial site to the final interstitial site. The migration barrier is 0.68 eV, which represents the energy difference between the initial point and saddle point. Due to the lower migration barrier value obtained here, Mo atom is easier to move by interstitial diffusion.

When vacancy defect exists (V_V or V_C) in the lattice, atoms can diffuse through the defect by occupying vacant site from their original position. From the analyses of defect complexes in Section 3.2, the following types of vacancy-assisted diffusion are unlikely to exist: (a) $I_{Mo} \rightarrow V_V$, (b) $I_{Mo} \rightarrow V_C$, (c) $S_{Mo-V} \rightarrow V_C$, (d) $S_{Mo-C} \rightarrow V_V$, and (e) $S_{Mo-C} \rightarrow V_C$. So the situation of substitution Mo atom (S_{Mo-V}) moving into the nearest V_V is calculated and shown in Figure 8B. The energy file for V_V-assisted Mo diffusion is similar to that of interstitial Mo diffusion, which is symmetric as well. However, the energy barrier of 5.07 eV is much larger than the value in Figure 8A, which means that the interstitial Mo diffusion path is energetically more favorable than the V_V-assisted one.

4 | DISCUSSION

Among all intrinsic defects in VC, V_C has the smallest formation energy for bulk material and only negative value for formation energy of defect, which means that V_C definitely exists in VC carbide, whereas all other point defects are not energetic favorable compared to perfect VC. In general, vacancy defect has the highest stability, then followed by interstitial and substitution defects, which are consistent with the results for ThC carbide with the same cubic structure,[25] but not with the stability trend in hexagonal WC.[22] Except for the substitution defects, C defects are accommodated much more easily than V defects for vacancy and interstitial defects, and many first-principles calculations for other TMCs have the exactly same conclusion with the results in this paper.[22,25,41]

It is already known that the formation energy for V_V is relatively large, so its stability is not so high. When V_V already exists in the crystal, free atoms have the tendency to enter the vacancy and fill the lattice as long as they can lower the formation energy and stabilize the structure. Free C atom is unlikely to fill V_V position forming S_C defect due to the higher formation energy than the structure only with V_V. While free Mo atom has high probability to enter into V_V position to form S_{Mo-V}, because the formation energy for S_{Mo-V} is significantly lower than that for V_V, which indicates that V_V in VC cell is easily occupied by free Mo atom. When extraneous Mo atom has already occupied V/C lattice or interstitial position, such

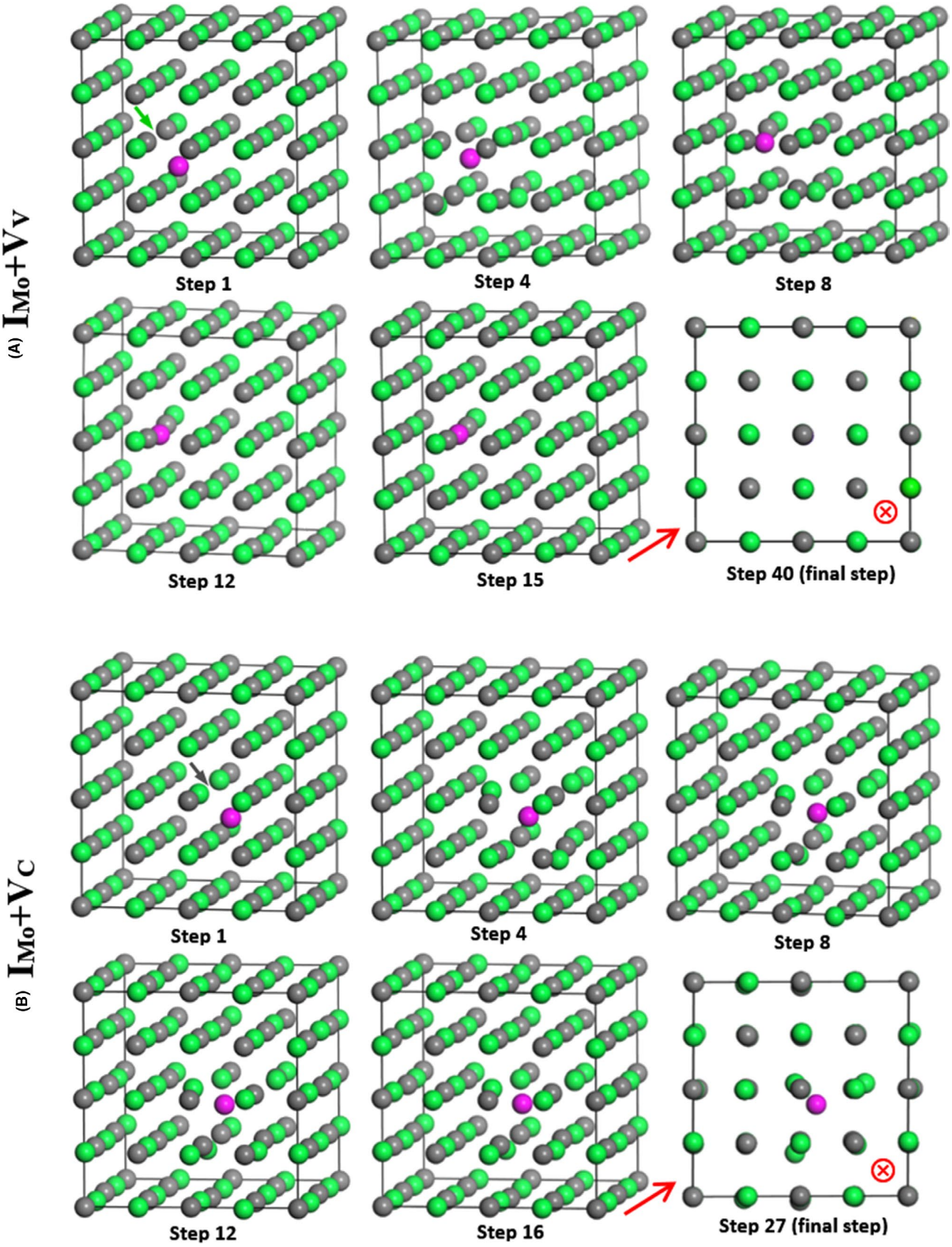

FIGURE 7 Structure evolution of VC supercell with (A) $I_{Mo} + V_V$ and (B) $I_{Mo} + V_C$ during optimization process. The green, gray, and purple balls represent V, C, and Mo atoms; the green and gray arrow in the first graph (Step 1) of (A) and (B) indicate the place where V_V and V_C locate; the last graphs in (A) and (B) are observed along the direction indicated by the red arrows [Color figure can be viewed at wileyonlinelibrary.com]

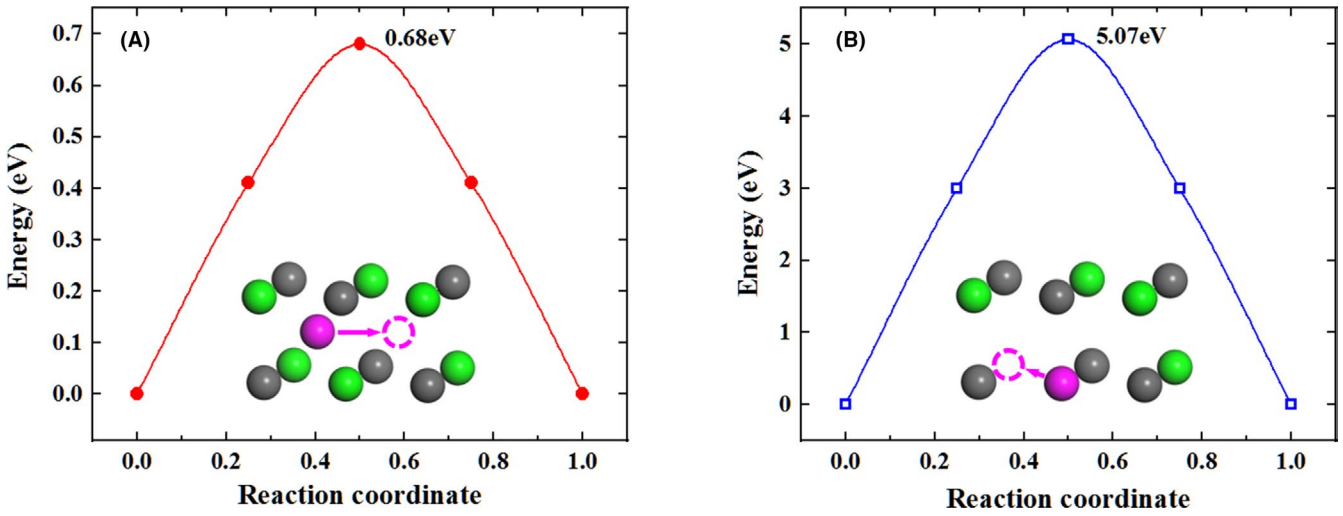

FIGURE 8 Calculated diffusion energy profiles of Mo atom diffusing along different diffusion ways in VC: (A) interstitial diffusion and (B) V_V-assisted diffusion [Color figure can be viewed at wileyonlinelibrary.com]

as in the case of $S_{Mo\text{-}V}$, $S_{Mo\text{-}C}$, and I_{Mo}, it is suggested from formation energy values that Mo atom in C lattice and interstitial Mo atom can enter the V_V position stabilizing the lattice structure. This also indicates that $S_{Mo\text{-}C} + V_V$ transforms into $S_{Mo\text{-}V} + V_C$ automatically during optimization process, which has been certified by Figure 7B, and these two defect complexes have almost identical formation energy values.

When V_C is present in the supercell, due to its extremely high stability, neither the free V or Mo atoms nor the existing Mo atoms in the lattice can occupy V_C position to form a more stable structure. So after considering the situation about S_V, $S_{Mo\text{-}C}$ and $S_{Mo\text{-}V} + V_C$ ($S_{Mo\text{-}C} + V_V$), VC carbide is found to tend to always exist in the form of nonstoichiometric VC_x ($x < 1$). In addition, the existence of V_C can stabilize the Mo-related defects ($S_{Mo\text{-}V}$, $S_{Mo\text{-}C}$, and I_{Mo}) in the lattice. It is found that the formation energies for structures with defect complexes $S_{Mo\text{-}V} + V_C$, $S_{Mo\text{-}C} + V_C$, and $I_{Mo} + V_C$ are all smaller than those without V_C.

For Mo-related defect complexes in VC system, the atom evolution during optimization process can be generally deduced according to the binding energy between two defects. Small binding energy (<1eV) shows the weak attraction between the defects, so Mo atom barely move in the lattice ($S_{Mo\text{-}V} + V_V$ and $S_{Mo\text{-}V} + V_C$). Large binding energy indicates that there is a certain attraction between two defects resulting in the displacement of Mo atom, so Mo atom tends to exist in the interstitial position ($S_{Mo\text{-}C} + V_C$ and $I_{Mo} + V_C$) after optimization. However, the binding energy values between defects discussed earlier are not fully matched with the formation energy values of defect complexes. Binding energy reveals the interaction between the defects and the trend of atom movement, whereas formation energy represents the stability of the final optimized structure. For example, both of the binding energies for $S_{Mo\text{-}V} + V_V$ and $S_{Mo\text{-}V} + V_C$ are small, which means the attraction between two defects in both of the complexes is not strong and the energy decrease in the system after the combination of two defects is not obvious. However, their formation energy values differ a lot from each other, and $S_{Mo\text{-}V} + V_C$ is found more stable than $S_{Mo\text{-}V} + V_V$.

VC is able to resist high temperature, high mechanical stress and intense radiation no matter as ceramic material or as precipitates in other metal-based materials in its applications, and a variety of point defects is inevitably formed in VC crystals. Among the three intrinsic defects studied in this paper, vacancy defects have the best stability. Through the analysis of Mo atom in VC, vacancy can provide sites for the existence and diffusion of other metal atoms at high temperature. When other alloy elements enter in the lattice and gradually accumulate, the performance of the entire VC crystal will surely change. In addition, metal atoms can stabilize the whole structure if they occupy the V sites in VC, so microalloying treatment can be considered for VC ceramics in production process. However, once the compositions are formed, the treatments under extreme conditions such as high temperature need to be adopted to achieve the interstitial diffusion for metal atoms in VC. Moreover, there must be V_C in VC crystal, but V_C cannot bind metal atoms in the lattice positions stably. Once metal atoms exist in the interstitial position, large lattice distortion will be generated due to the size effect improving the performance of ceramic materials to some extent.

5 | CONCLUSION

1. The existence of V_V leads to the shrinkage of the crystal structure, whereas V_C causes slightly volume expansion after optimization. Substitution defects S_V and S_C mainly influences the nearest atom position D_{1N} in the lattice, and I_V is found to have more obvious lattice change than I_C. In addition, Mo-related defect $S_{Mo\text{-}V}$ will not affect lattice

constants markedly, but $S_{Mo\text{-}C}$ will due to the similar character for Mo to the neighboring V atoms. The volume change for I_{Mo} is the largest among all the supercells with defects.
2. V_C is the most stable defect that can exist in the structure and all other point defects are not energetic favorable compared to perfect VC. Moreover, C defects are accommodated much more easily than V defects for vacancy and interstitial defects.
3. In general, Mo-related defects are less stable than intrinsic ones expect $S_{Mo\text{-}V}$. Free Mo atoms have the tendency to occupy the lattice position of V atoms and exist more stable than already formed V_V.
4. Both vacancy defect and substitution defect weaken the electron-gaining/losing capacity of the nearest atoms. For substitution defect and interstitial defect, the defect atom gains/losses less electrons than normal atoms, among which atomic charge of C defect atom for S_C is only −0.05 and the interstitial V atom for I_V nearly shows no electron transfer. I_C is the only condition that make V atoms nearby lose more electrons among all intrinsic defects. For Mo-related defects, substitution Mo atom exhibits much worse ability of losing electron for both $S_{Mo\text{-}V}$ and $S_{Mo\text{-}C}$, whereas interstitial Mo atom even shows the characteristic of gaining electrons.
5. Due to the stability of $S_{Mo\text{-}V}$, the values of binding energy for $S_{Mo\text{-}V} + V_V$ and $S_{Mo\text{-}V} + V_C$ defect complexes are very small showing the weak attraction between $S_{Mo\text{-}V}$ and V_V/V_C. Large binding energy makes Mo atom in $S_{Mo\text{-}C} + V_C$ and $I_{Mo} + V_C$ tends to exist in the interstitial position after optimization.
6. The possible diffusion path for Mo atom includes interstitial diffusion and V_V-assisted diffusion. The energetically most favorable migration path for Mo atom is through the interstitial one.

ACKNOWLEDGMENTS

The authors express their gratitude for projects supported by the European Union's Horizon 2020 Research and Innovation Programme under the Marie Skłodowska-Curie grant agreement (No. 793114) and National Natural Science Foundation of China (51674123). The authors also thank Yang Zhang, Jago Tomos Reed-Jones and Novoth Szilárd for their support in useful discussions.

ORCID

Jing Guo https://orcid.org/0000-0002-3349-8568

REFERENCES

1. Aizawa T, Souda R, Otani S, Ishizawa Y, Oshima C. Anomalous bond of monolayer graphite on transition-metal carbide surfaces. Phys Rev Lett. 1990;64:768–71.
2. Yang J, Ye Z, Huang JH, Chen SH, Zhao Y. First-principles calculations on wetting interface between Ag-Cu-Ti filler metal and SiC ceramic: Ag(111)/SiC(111) interface and Ag(111)/TiC(111) interface. Appl Surf Sci. 2018;462:55–64.
3. Yang J, Huang JH, Fan DY, Chen SH. First-principles investigation on the electronic property and bonding configuration of NbC(111)/NbN(111) interface. J Alloy Compd. 2016;689:874–84.
4. Guo J, Liu L, Liu S, Zhou Y, Qi X, Ren X, et al. Stability of eutectic carbide in Fe-Cr-Mo-W-V-C alloy by first-principles calculation. Mater Des. 2016;106:355–62.
5. Wu L, Yao T, Wang Y, Zhang J, Xiao F, Liao B. Understanding the mechanical properties of vanadium carbides: Nano-indentation measurement and first-principles calculations. J Alloy Compd. 2013;548:60–4.
6. Takahashi J, Kawakami K, Kobayashi Y. Origin of hydrogen trapping site in vanadium carbide precipitation strengthening steel. Acta Mater. 2018;153:193–204.
7. Kaneko M, Doshida T, Takai K. Changes in mechanical properties following cyclic prestressing of martensitic steel containing vanadium carbide in presence of nondiffusible hydrogen. Mater Sci Eng A. 2016;674:375–83.
8. Ioannidou C, Arechabaleta Z, Navarro-López A, Rijkenberg A, Dalgliesh RM, Kölling S, et al. Interaction of precipitation with austenite-to-ferrite phase transformation in vanadium micro-alloyed steels. Acta Mater. 2019;181:10–24.
9. Li H, Tong W, Cui J, Zhang H, Chen L, Zuo L. The influence of deep cryogenic treatment on the properties of high-vanadium alloy steel. Mater Sci Eng A. 2016;662:356–62.
10. Cao H, Dong X, Chen S, Dutka M, Pei Y. Microstructure evolutions of graded high-vanadium tool steel composite coating in-situ fabricated via atmospheric plasma beam alloying. J Alloy Compd. 2017;720:169–81.
11. Zou Y, Ma B, Cui H, Lu F, Xu P. Microstructure, wear, and oxidation resistance of nanostructured carbide-strengthened cobalt-based composite coatings on Invar alloys by laser cladding. Surf Coat Tech. 2020;381:125188.
12. Gualtieri T, Bandyopadhyay A. Additive manufacturing of compositionally gradient metal-ceramic structures: stainless steel to vanadium carbide. Mater Des. 2018;139:419–28.
13. Guo J, Liu LG, Li Q, Sun Y, Gao Y, Ren X, et al. Characterization on carbide of a novel steel for cold work roll during solidification process. Mater Charact. 2013;79:100–9.
14. Lin N, Zhao L, Zou J, Ma C, Wang Z, He Y. Improvement in densification process and properties of Ti(C, N)-based cermets with vanadium carbide addition. Ceram Int. 2019;45:2692–700.
15. Günen A, Kurt B, Milner P, Gök MS. Properties and tribological performance of ceramic-base chromium and vanadium carbide composite coatings. Int J Refract Met H. 2019;81:333–44.
16. Cai X, Xu Y, Liu M. Growth kinetics and mechanical properties of the V2C and V8C7 carbide layers on iron substrate. Surf Coat Tech. 2020;382:125148.
17. Guo J, Liu L, Feng Y, Liu S, Ren X, Yang Q. Crystallographic characterizations of eutectic and secondary carbides in a Fe-12Cr-2.5Mo-1.5W-3V-1.25C alloy. Met Mater Int. 2017;23:313–9.
18. Ren X. Large electric-field-induced strain in ferroelectric crystals by point-defect-mediated reversible domain switching. Nat Mater. 2004;3:91–4.
19. Wang C, Xing Y, Xia Y. Effect of vacancy defects on electronic properties and wettability of coal surface. Appl Surf Sci. 2020;511:145546.
20. Liu M, WangS WC. Understanding of electronic and optical properties of ZnS with high concentration of point defects induced by

hot pressing process: the first-principles calculations. Comp Mater Sci. 2020;174:109492.
21. Burr PA, Oliver SX. Formation and migration of point defects in tungsten carbide: unveiling the sluggish bulk self-diffusivity of WC. J Eur Ceram Soc. 2019;39:165–72.
22. Kong XS, You YW, Xia JH, Liu CS, Fang QF, Luo GN, et al. First principles study of intrinsic defects in hexagonal tungsten carbide. J Nucl Mater. 2010;406:323–9.
23. Sun W, Ehteshami H, Kent PRC, Korzhavyi PA. Self-diffusion of Ti interstitial based point defects and complexes in TiC. Acta Mater. 2019;165:381–7.
24. Razumovskiy VI, Popov MN, Ding H, Odqvist J. Formation and interaction of point defects in group IVb transition metal carbides and nitrides. Comp Mater Sci. 2015;104:147–54.
25. Daroca DP, Jaroszewicz S, Llois AM, Mosca HO. First-principles study of point defects in thorium carbide. J Nucl Mater. 2014;454:217–22.
26. Gusev AI. Effect of carbon vacancies on the electric resistivity of nonstoichiometric VCy vanadium carbide. JETP Lett. 2009;90:191–6.
27. Gusev AI, Kurlov AS, Rempel AA. Domains of the phases V8C7 and V3C2 in bulk carbide VCy. JETP Lett. 2015;101:533–8.
28. Kurlov AS, Gusev AI. Effects of nonstoichiometry and ordering on the basic lattice constant of vanadium carbide VCy. JETP Lett. 2017;101:357–63.
29. Kurlov AS, Gusev AI. Effect of nonstoichiometry on the lattice constant of cubic vanadium carbide VCy. Phys Solid State. 2017;59:1520–5.
30. Ghasali E, Ebadzadeh T, Alizadeh M. Mechanical and microstructural properties of WC-based cermets: a comparative study on the effect of Ni and Mo binder phases. Ceram Int. 2018;44:2283–91.
31. Guo J, Ai L, Wang T, Feng Y, Wan D, Yang Q. Microstructure evolution and micro-mechanical behavior of secondary carbides at grain boundary in a Fe-Cr-W-Mo-V-C alloy. Mater Sci Eng A. 2018;715:359–69.
32. Hohenberg P, Kohn W. Inhomogeneous electron gas. Phys Rev B. 1964;136:864–71.
33. Sun S, Li C, Zhang D, Wang Y. Density functional theory study of the adsorption and dissociation of O_2 on CuO(1 1 1) surface. Appl Surf Sci. 2015;333:229–34.
34. Cao LZ, Shen J, Chen NX. Theoretical study of the phase stability and site preference for $R_3(Fe, T_{)2}9$ (R = Nd, Sm; T = V, Ti, Cr, Cu, Nb, Mo, Ag). J Alloy Compd. 2002;336:18–28.
35. Mardirossian N, Head-Gordon M. Mapping the genome of meta-generalized gradient approximation density functionals: the search for B97M-V. J Chem Phys. 2015;142:A1133–A1138.
36. Kim S, Szlufarska I, Morgan D. Ab initio study of point defect structures and energetics in ZrC. J Appl Phys. 2010;107:053521.
37. Politi JRS, Viñes F, Rodriguez JA, Illas F. Atomic and electronic structure of molybdenum carbide phases: bulk and low Miller-index surfaces. Phys Chem Chem Phys. 2013;15:12617–25.
38. Lipatnikov VN, Gusev AI, Ettmayer P, Lengauer W. Phase transformations in non-stoichiometric vanadium carbide. J Phys: Condens Mat. 1999;11:163–84.
39. Burdett JK, Mitchell JF. Nonstoichiometry in early transition metal compounds with the rocksalt structure. Prog Solid State Ch. 1995;23:131–70.
40. Zhang P, Zou T, Feng S. First principles investigations of hydrogen interaction with vacancy-oxygen complexes in vanadium alloys. Int J Hydrogen Energ. 2019;44:26637–45.
41. Yang XY, Lu Y, Zhang P. First-principles study of native point defects and diffusion behaviors of helium in zirconium carbide. J Nucl Mater. 2015;465:161–6.

SUPPORTING INFORMATION

Additional supporting information may be found online in the Supporting Information section.

How to cite this article: Guo J, Feng Y, Tang C, Ren X. Intrinsic defects, Mo-related defects, and complexes in transition-metal carbide VC: A first-principles study. *J Am Ceram Soc*. 2020;103:7226–7239. https://doi.org/10.1111/jace.17411